LBL-3393 c.2
UC-32 Mathematics
and Computers
TID-4500-R62

VORTEX BLOBS IN A SQUARE CAVITY
APPLICATION OF CHORIN'S METHOD

Aleksei Ilyich Shestakov

October 1974

Prepared for the U. S. Atomic Energy Commission
under Contract W-7405-ENG-48

TWO-WEEK LOAN COPY

This is a Library Circulating Copy which may be borrowed for two weeks. For a personal retention copy, call Tech. Info. Division, Ext. 5545

LAWRENCE BERKELEY LABORATORY
UNIVERSITY OF CALIFORNIA
BERKELEY

LBL-3393 c.2

DISCLAIMER

This document was prepared as an account of work sponsored by the United States Government. While this document is believed to contain correct information, neither the United States Government nor any agency thereof, nor the Regents of the University of California, nor any of their employees, makes any warranty, express or implied, or assumes any legal responsibility for the accuracy, completeness, or usefulness of any information, apparatus, product, or process disclosed, or represents that its use would not infringe privately owned rights. Reference herein to any specific commercial product, process, or service by its trade name, trademark, manufacturer, or otherwise, does not necessarily constitute or imply its endorsement, recommendation, or favoring by the United States Government or any agency thereof, or the Regents of the University of California. The views and opinions of authors expressed herein do not necessarily state or reflect those of the United States Government or any agency thereof or the Regents of the University of California.

Table of Contents

1. Introduction 1
2. Equations of Motion and Statement of Problem 2
3. Chorin's Scheme-Overview 4
4. Potential Flow 8
   4.0. Statement of problem and definitions 8
   4.1. Numerical method of Solution 9
   4.2. Construction of spline interpolator 11
      4.2a. One dimensional case 11
      4.2b. Two dimensional case 12
   4.3 Linear equations for the spline coefficients 15
   4.4. Solution of system for the spline coefficients 20
   4.5. Timing tests for the potential flow calculation 26
5. Numerical Experiment and Results. 27
6. Discussion of Results 37
7. Discussion of Program-Conclusion 38
8. References 40

VORTEX BLOBS IN A SQUARE CAVITY APPLICATION OF CHORIN'S METHOD

Aleksei Ilyich Shestakov

Lawrence Berkeley Laboratory
and
Lawrence Livermore Laboratory
University of California
Berkeley, California 94720

October 1974

ABSTRACT

Chorin's method of solution of the Navier-Stokes equations, using vorticity blobs receiving both a deterministic as well as a random push, is applied to the two-dimensional problem of a flow inside a square cavity where one side moves in its own plane with a unit velocity. Results are presented for a Reynolds number of 10^3.

1. Introduction

The problem of computing the two-dimensional flow in a square cavity has enjoyed much popularity in the fields of Numerical Analysis and Fluid Dynamics. This popularity has been responsible for the extensive literature on the subject. The problem is often used as a model to test numerical techniques on flows containing closed streamlines.

To my knowledge, all of the schemes found in the literature approximate the derivatives by divided differences of function values computed on a predesignated mesh over the domain. This seems to impose an upper bound on the Reynolds number that one can use, since analysis implies that at least several grid points must fall within the boundary layer whose thickness is $\mathcal{O}(R^{-1/2})$.

Chorin's scheme [7] is grid-free and seems to simulate the actual physics of the problem; it is essentially an application of the finite element method in Lagrangian coordinates. It is this scheme which is presented and applied in this report.

2. Equations of Motion and Statement of Problem

In the following, vectors and vector operators will be underlined, e.g., $\underline{u}$, $\underline{\nabla}$ denote the vector $\underline{u}$ and the gradient operator; while scalar functions will be denoted by letters, e.g., ζ.

The equations of interest are the Navier-Stokes equations for two-dimensional flow, written in the vorticity transport form,

$$\partial_t \zeta + \underline{u} \cdot \underline{\nabla} \zeta = \frac{1}{R} \Delta \zeta . \tag{1}$$

ζ is the vorticity, $\underline{u} = (u, v)$ is the velocity vector, and R is the Reynolds number. Since the flow is two-dimensional and incompressible, there exists a stream function ψ, related to ζ by

$$\Delta \psi = - \zeta , \tag{2}$$

where $\Delta \equiv \partial^2/\partial x^2 + \partial^2/\partial y^2$ is the Laplacian operator. The velocity vector, $\underline{u}$, can then be expressed in terms of ψ by,

$$\underline{u} = (u, v) = (\partial_y \psi, - \partial_x \psi), \tag{3}$$

where u, v are the horizontal, and vertical components of $\underline{u}$. Using (2) and (3), it follows that,

$$\underline{\nabla} \times \underline{u} = \zeta ,$$

i.e., the curl of the velocity is the vorticity. Equations (1), (2), and (3) are to be solved in a domain $\mathcal{D}$ with the imposed "no slip" condition at the boundary, $\partial \mathcal{D}$,

$$\underline{u} = \text{velocity of the boundary}, \tag{4}$$

or if the boundary does not move,

$$\underline{u} = 0 \quad \text{at} \quad \partial \mathcal{D}.$$

There is also a specified initial condition,

$$\underline{u}(t = 0) = \underline{u}_0 , \text{ given.}$$

In particular, consider the problem of computing the flow inside a square cavity with the specified boundary conditions, (Fig. 1) and the initial condition $\underline{u} = (0, 0)$ in $\mathcal{D}$. The problem is to compute the steady flow inside the cavity when the bottom edge has impulsively started to move in its own plane, to the right, with unit velocity.

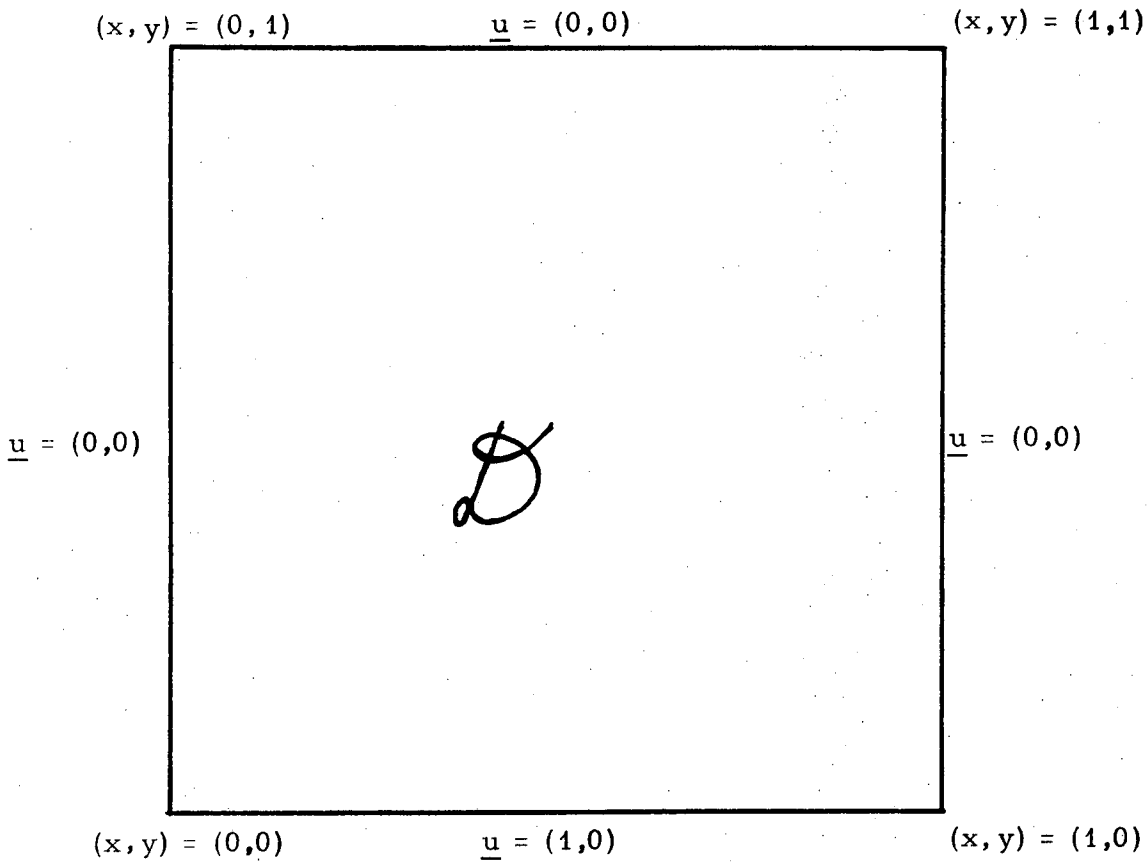

Fig. 1. Domain of interest and boundary conditions.

3. Chorin's Scheme-Overview

In this section an outline of Chorin's vortex scheme is presented, [7].

Consider the problem of computing the evolution of vorticity governed by Eqs. (1), (2), (3), and the boundary condition Eq. (4). Chorin assumes that the vorticity is a sum of blobs, or vortices,

$$\zeta(\underline{r}) = \sum_j \zeta_j(\underline{r}-\underline{r}_j), \tag{5}$$

where each $\zeta_j(\underline{r})$ is a radially symmetric function of small support, and $|\underline{r}| = \sqrt{x^2 + y^2}$. Derive a velocity field, $\underline{u}_\zeta(\underline{r})$, induced by this distribution of vorticity by solving Eqs. (2) and (3). If each vortex blob has attached to it a strength ζ_j, then we have a new representation for the vorticity,

$$\zeta(\underline{r}) = \sum_j \zeta_j \zeta_0(\underline{r}-\underline{r}_j) \tag{6}$$

where,

$$\zeta_0(\underline{r}) = \begin{cases} \dfrac{1}{2\pi\sigma r} & , \ r < \sigma \\ 0 & , \ r \geq \sigma \ . \end{cases} \tag{7}$$

The constant σ is the <u>cut-off length</u>, to be determined shortly, and $r = |\underline{r}|$. The expression for ζ_0 will become convincing if we consider the integral of the vorticity,

$$\iint_{\mathcal{D}} \zeta(x,y)dxdy = \iint_{\mathcal{D}} \sum_j \zeta_j \zeta_0(\underline{r}-\underline{r}_j)\underline{dr} = \Sigma\zeta_j,$$

where the integral has been evaluated using polar coordinates. Equation (7) will also make more sense after the discussion on the generation of vorticity.

The basic vortex $\zeta_0(\underline{r})$ in turn generates its own blob stream function, $\psi_0(\underline{r})$; by solving,

$$\Delta\psi_0 = -\zeta_0$$

neglecting boundary values for the moment,

$$\psi_0(\underline{r}) = \begin{cases} -\dfrac{1}{2\pi} \log r, & r \geq \sigma \\ -\dfrac{1}{2\pi\sigma} r & , \ r < \sigma \ . \end{cases} \tag{8}$$

Using Eqs. (8), (3) and (6), a velocity field,

$$\underline{u}_\zeta(x,y) = \sum_j \zeta_j \, \underline{u}_0(x-x_j,\ y-y_j) \tag{9}$$

is induced by the vorticity. In Eq. (9), $\underline{u}_0$ is the velocity induced by a single vortex located at the origin, and (x_j, y_j) is the location of the $j^{\underline{th}}$ vortex. $\underline{u}_0(x,y)$ is obtained by differentiating (Eq. 8),

$$\underline{u}_0(x,y) = (\partial_y \psi_0,\ -\partial_x \psi_0) = \begin{cases} \dfrac{1}{2\pi r^2}\,(-y,x), & r \geq \sigma \\[2ex] \dfrac{1}{2\pi\sigma r}\,(-y,x), & r < \sigma . \end{cases} \tag{9.5}$$

$\underline{u}_\zeta$ is a continuous velocity field obtained from a discontinuous, in fact singular, distribution of vorticity.

It is possible (Davari [13]), to generate a continuous stream function, ψ_0, by the addition of a constant, which yields

$$\psi_0(\underline{r}) = \begin{cases} -\dfrac{1}{2\pi}\log r & , r \geq \sigma \\[2ex] \dfrac{1}{2\pi}\left(1 - \log\sigma - \dfrac{r}{\sigma}\right), & r < \sigma , \end{cases} \tag{8.5}$$

and it is the expression (Eq. 8.5) which is used by the computer program.

The actual solution of Eq. (1) is obtained by a first order correct in time, differencing algorithm which uses no spatial grid, but merely keeps track of the centers of the vortices.

The velocity field $\underline{u}_\zeta$ does not satisfy any boundary conditions. Section 4 will explain how, using $\underline{u}_\zeta$, an irrotational velocity field $\underline{u}_p$ (i.e. $\underline{\nabla} \times \underline{u}_p = 0$) is constructed such that the combined velocity $\underline{u} \equiv \underline{u}_\zeta + \underline{u}_p$ satisfies

$$\underline{u} \cdot \underline{n} = \underline{u}_p \cdot n + \underline{u}_\zeta \cdot \underline{n} = 0 \quad \text{at } \partial\mathcal{D},$$

where $\underline{n}$ is the normal velocity vector at the boundary. Postponing the discussion regarding the second boundary condition ($\underline{u} \cdot \underline{s} = 0$), let $\underline{u}$ denote the velocity field satisfying the normal boundary condition.

Equation (1) is solved in two steps. The vortices move according to two distinct laws; the first, the deterministic component is Euler's equation.

$$\partial_t \zeta + (\underline{u} \cdot \underline{\nabla})\zeta = 0 \tag{10}$$

or if we follow the particles of the fluid,

$$\frac{D\zeta}{Dt} = 0; \tag{10.5}$$

and the second is the diffusive component,

$$\partial_t \zeta = \frac{1}{R} \Delta\zeta \ . \tag{11}$$

Equation (10), or (10.5), is solved by keeping track of the locations of the vortices. If (x_i, y_i) denotes the position of the i-th vortex then,

$$\frac{d}{dt}(x_i, y_i) = \sum_{j \neq i} \zeta_j \, \underline{u}_0(x_i - x_j, y_i - y_j) + \underline{u}_p(x_i, y_i) \tag{12}$$

or, if (x_i^m, y_i^m) in the location of the i-th vortex at the m-th time step,

$$\begin{aligned} &(x_i^{m+1}, y_i^{m+1}) \\ &= (x_i^m, y_i^m) + k \left[\sum_{j \neq i} \zeta_j \underline{u}_0(x_i^m - x_j^m, y_i - y_j^m) + u_p(x_i^m, y_i^m) \right], \end{aligned} \tag{13}$$

where k is the time step. This is Euler's method for the solution of ordinary differential equations.

Equation (11) is solved by the random walk method developed by Chorin [7], whose idea was described by Courant, Friedricks, and Lewy [8] in their classic paper on difference schemes. If $\underline{\eta} = (\eta_1, \eta_2)$ is a vector whose components are gaussianly distributed random variables, with mean zero and variance $2k/R$, then Eq. (11) is approximated by

$$(x_i^{m+1}, y_i^{m+1}) = (x_i^m, y_i^m) + (\eta_1, \eta_2). \tag{14}$$

Denoting the right hand side of Eq. (12) by $\underline{u}^m$, then Eqs. (13) and (14) are combined to yield,

$$(x_i^{m+1}, y_i^{m+1}) = (x_i^m, y_i^m) + k \, \underline{u}^m + (\eta_1, \eta_2) \tag{15}$$

as the approximation to Eq. (1).

Consider now the generation of vorticity at the boundary. As previously noted, the field $\underline{u}$ does not satisfy the tangential boundary condition,

$\underline{u}\cdot\underline{s} = 0$ or the tangential boundary velocity component, where $\underline{s}$ is the unit vector tangential to $\partial\mathcal{D}$. To correct this deficiency, imagine the existence of a thin, viscous, boundary layer. To evaluate the vorticity present, simply integrate $\underline{\nabla}\times\underline{u}$ in the boundary layer. If the boundary is broken up into segments of length h, and one uses a midpoint rule approximation to the integral, the vorticity in the boundary layer of width δ and length h (see Fig. 2),

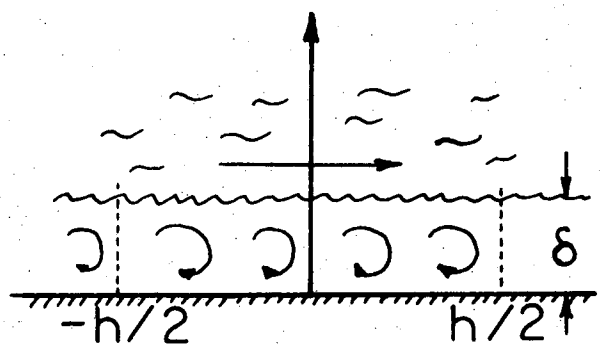

Fig. 2. Boundary layer along a wall.

is,

$$\int_{-h/2}^{h/2}\int_{0}^{\delta}(\underline{\nabla}\times\underline{u})\,dydx = \int_{-h/2}^{h/2}\int_{0}^{\delta}(-\partial_y u)dydx \simeq -\,u(0,\delta)\times h. \qquad (16)$$

$u(0,\delta)$ is the free stream velocity at the edge of the boundary layer, and it is set equal to $u(0,0)$, the velocity component at the boundary one wants to cancel. Note that above calculation was done using a local coordinate system. This vorticity is then coagulated into a new vortex. The newly created vorticity is allowed to diffuse, and it is the shape of the diffusing vortex, inside the cut-off length, which now exerts a constant velocity at the boundary equal to the negative of $\underline{u}\cdot\underline{s}$. This accomplishes the cancellation of the tangential boundary component and gives a value for σ, namely $\sigma = h/2\pi$. The new vortices diffuse into $\mathcal{D}$ and become a part of the field ζ. The entire process is then reiterated.

4. Potential Flow

4.0. Statement of problem and definitions.

In order to move the vortices, it is necessary to have a velocity field which satisfies the normal boundary condition; i.e. if the vortices are moved according to a velocity $\underline{u}$, then $\underline{u}$ must satisfy

$$\underline{u}\cdot\underline{n} = 0 \quad \text{at } \partial\mathcal{D}. \tag{17}$$

If $\underline{u}_\zeta$ is the velocity field generated by the vortices,

$$\underline{u}_\zeta(\underline{r}) = \sum_j \zeta_j\, \underline{u}_0(\underline{r}-\underline{r}_j),$$

where $\underline{u}_0(\underline{r})$ is given by Eq. (9.5), then a velocity $\underline{u}_p$ is constructed, such that

$$\underline{u}_p\cdot\underline{n} = -\,\underline{u}_\zeta\cdot\underline{n} \quad \text{at} \quad \partial\mathcal{D}. \tag{18}$$

Certainly, no extra vorticity should be added to the fluid, so $\underline{u}_p$ also satisfies,

$$\underline{\nabla}\times\underline{u}_p = 0 \quad \text{in } \mathcal{D}. \tag{19}$$

Then defining $\underline{u} \equiv \underline{u}_p + \underline{u}_\zeta$, Eq. (17) is satisfied.

To calculate $\underline{u}_p$, assume the existence of a sufficiently differentiable function $\psi_p = \psi_p(x,y)$ such that,

$$\underline{u}_p = (\partial_y\psi_p,\ -\,\partial_x\psi_p). \tag{20}$$

In this manner, the problem defined by Eqs. (18) and (19) is transformed into the classical Dirichlet problem of Potential Theory. Using Eq. (8.5) construct the stream function of the vortices,

$$\psi_\zeta(\underline{r}) = \sum_j \zeta_i\, \psi_0(\underline{r}-\underline{r}_j), \tag{21}$$

and at the boundary set

$$\psi_p(s) = -\,\psi_\zeta(s) \qquad (\text{on } \partial\mathcal{D}); \tag{22}$$

while, using Eqs. (19) and (20),

$$\Delta\psi_p = 0 \quad \text{in } \mathcal{D}. \tag{23}$$

It is the solution of Eq. (23) using Eq. (22) which is discussed in this section.

Defining,

$$\psi \equiv \psi_p + \psi_\zeta \tag{24}$$

as the stream function of the flow, Eq. (22) sets the $\psi = 0$ streamline on the boundary. Since

$$0 = \frac{\partial \psi}{\partial s} = \underline{u} \cdot \underline{n}$$

the generation of a velocity field satisfying the normal boundary condition is accomplished.

4.1. Numerical method of solution

Numerically, the potential flow problem is solved as follows: Choose an integer ℓ, e.g. $\ell = 5$, and define $N \equiv 2^{\ell+1} - 1$. Define $d \equiv 1/(N+1)$, and impose a square grid on $\mathcal{D}$ of mesh size d (Fig. 3).

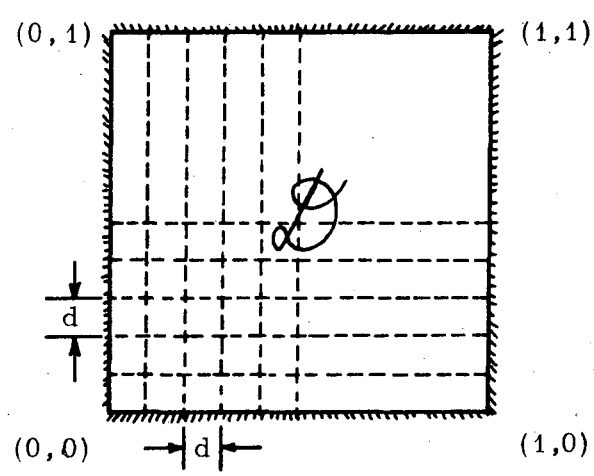

Fig. 3. Square mesh for calculation of potential flow.

Let $\psi_{i,j}$ be an approximation to $\psi_p(jd, id)$; then using a standard 5-pt. approximation to the Laplacian operator, the equation

$$\frac{\partial^2}{\partial x^2} \psi_p(jd, id) + \frac{\partial^2}{\partial y^2} \psi_p(jd, id) = 0$$

becomes,

$$(\psi_{i+1,j} + \psi_{i,j+1} + \psi_{i-1,j} + \psi_{i,j-1} - 4\,\psi_{i,j})/d^2 = 0, \quad \text{or simply,}$$

$$\psi_{i-1,j} + \psi_{i,j-1} - 4\psi_{i,j} + \psi_{i,j+1} + \psi_{i+1,j} = 0,$$

and the values of any boundary mesh points are evaluated using Eq. (22).

Hence, the partial differential equation, $\Delta\psi = 0$, is transformed into the matrix equation $F\Psi = \underline{y}$ where F is block tridiagonal,

$$F = \begin{bmatrix} \Gamma & I & & & & \\ I & \Gamma & I & & & \\ & I & \Gamma & I & & \\ & & I & \cdot & \cdot & \\ & & & \cdot & \cdot & \cdot \\ & & & & \cdot & \Gamma \end{bmatrix},$$

I is the unit diagonal matrix, and Γ is tridiagonal,

$$\Gamma = \begin{bmatrix} -4 & 1 & & & & \\ 1 & -4 & 1 & & & \\ & 1 & -4 & 1 & & \\ & & 1 & \cdot & \cdot & \\ & & & \cdot & \cdot & \cdot \\ & & & & \cdot & \cdot \end{bmatrix},$$

$\Psi = (\Psi^{(1)}, \Psi^{(2)}, \ldots, \Psi^{(N)})^T$, and $\Psi^{(\ell)} = (\psi_{\ell,1}, \psi_{\ell,2}, \cdots, \psi_{\ell,N})^T$, for $\ell = 1, 2, \cdots, N$. The vector $\underline{y}$ is of dimension N^2 and contains many zeroes as well as the boundary values of ψ_p in its corresponding positions.

The system $F\Psi = \underline{y}$ is solved using the Buneman variant, of the odd-even cyclic reduction algorithm [6], and the solution is an approximation to the potential stream function, ψ_p, at the grid points of the imposed mesh.

To obtain a numerical function ψ_p which can be evaluated and differentiated <u>anywhere,</u> the computed mesh function Ψ is approximated by a bi-quadratic spline function $f(x,y)$, which is continuously differentiable and defined everywhere in $\mathcal{D} \cup \partial\mathcal{D}$. The numerical details of the evaluation of the spline function are found in the next section.

In conclusion, the spline function f is a bi-quadratic continuously differentiable function which is an approximation to the grid function Ψ which

solves $F\Psi = \underline{y}$, the matrix equation approximating $\Delta\psi_p = 0$. To evaluate $\underline{u}_p$,

$$\underline{u}_p \equiv (\partial_y f, -\partial_x f).$$

4.2. Construction of spline interpolator (Ref. [4])

4.2a. One-dimensional case: Assume the $\{y_i\}$ is an array of function values on a grid, i.e. $y_i = y(x_j)$, and that the points $\{x_j\}$ are equally spaced, (Fig. 4)

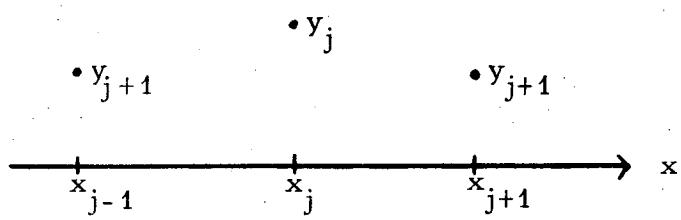

Fig. 4. Discrete function values of $y = y(x)$.

i.e. for all j, $|x_j - x_{j+1}| = d$. Then, for all x, $\exists, |x - x_j| \leq d/2$, define the spline interpolator,

$$f(x) = g_j + \delta_0 g_j x + \frac{1}{2}\left(x^2 + \frac{d^2}{4}\right)\delta_0^2 g_j .$$

It is tacitly assumed in the above definition that $x_j = 0$; if not, then substitute $x - x_j$ for x. The operators δ_0 and δ_0^2 are the first and second central difference operators on the spline coefficients $\{g_j\}$, i.e.

$$\delta_0 g_j \equiv \frac{1}{2d}(g_{j+1} - g_{j-1}) \text{ and } \delta_0^2 g_j \equiv \frac{1}{d^2}(g_{j+1} - 2g_j + g_{j-1}),$$

or in other words,

$$f(x) = \frac{1}{8}(g_{j-1} + 6g_j + g_{j+1}) + \frac{x}{2d}(g_{j+1} - g_{j-1})$$
$$+ \frac{1}{2}\frac{x^2}{d^2}(g_{j+1} - 2g_j + g_{j-1}).$$

Derive relationships for the spline coefficients by requiring that the spline agree with the given values y_i at the points x_j, i.e.

$$y_j = f(x_j) = \frac{1}{8}(g_{j-1} + 6g_j + g_{j+1}). \tag{25}$$

Equation (25) becomes a tridiagonal system for the spline coefficients g_j, and having solved for the g_j's, to evaluate the spline, one need only look up 3 spline coefficients in a table, namely $g_{j \pm 1}$, and g_j.

4.2.b. Two dimensional case: Assume that there is a square mesh of mesh size d imposed on the domain and that $\psi_{i,j}$ is an approximation to $\psi_p(jd, id)$, the stream function of the potential flow. There are a total of N interior points in each direction, so Ψ is an array of N^2 elements.

The problem is to find continuous functions approximating the derivatives of ψ_p at points (x, y), where (x, y) does not necessarily coincide with a mesh point. Assume for simplicity that $|x - x_j|$, $|y - y_i| \leq d$ and $(x_j, y_i) = (0, 0)$. Then the spline interpolator is:

$$f(x,y) \equiv g_j^{(i)}(y) + \delta_{0j} g_j^{(i)}(y)\, x + \frac{1}{2}\left(x^2 + \frac{d^2}{4}\right) \delta_{0j}^2 g_j^{(i)}(y)$$

where,

$$\delta_{0j} g_j^{(i)}(y) \equiv \frac{1}{2d}\left[g_{j+1}^{(i)}(y) - g_{j-1}^{(i)}(y)\right]$$

and

$$\delta_{0j}^2 g_j^{(i)}(y) \equiv \frac{1}{d^2}\left[g_{j+1}^{(i)}(y) - 2\, g_j^{(i)}(y) + g_{j-1}^{(i)}(y)\right] \tag{26}$$

are the first and second central differences of $g_j^{(i)}(y)$ on the index j. The function $g_j^{(i)}(y)$ is the one-dimensional spline in the vertical (y) direction around $y = y_i$, at the point $x = x_j$;

$$g_j^{(i)}(y) = \frac{1}{8}\left(f_{i+1,j} + 6 f_{i,j} + f_{i-1,j}\right) + \frac{y}{2d}\left(f_{i+1,j} - f_{i-1,j}\right)$$

$$+ \frac{1}{2}\frac{y^2}{d^2}\left(f_{i+1,j} - 2 f_{i,j} + f_{i-1,j}\right). \tag{27}$$

Once the coefficients $f_{i,j}$ have been computed, to evaluate the spline it is necessary to look up in a table the nine spline coefficients $f_{i,j}$, $f_{i\pm1,j\pm1}$, $f_{i,j\pm1}$, and $f_{i\pm1,j}$. The table of spline coefficients can be stored over the old function values since they are now superfluous.

There are, however, a few more spline coefficients than original function values. Initially there were N^2 interior function values $\psi_{i,j}$ and 4(N+1) boundary values ψ_s (Fig. 5).

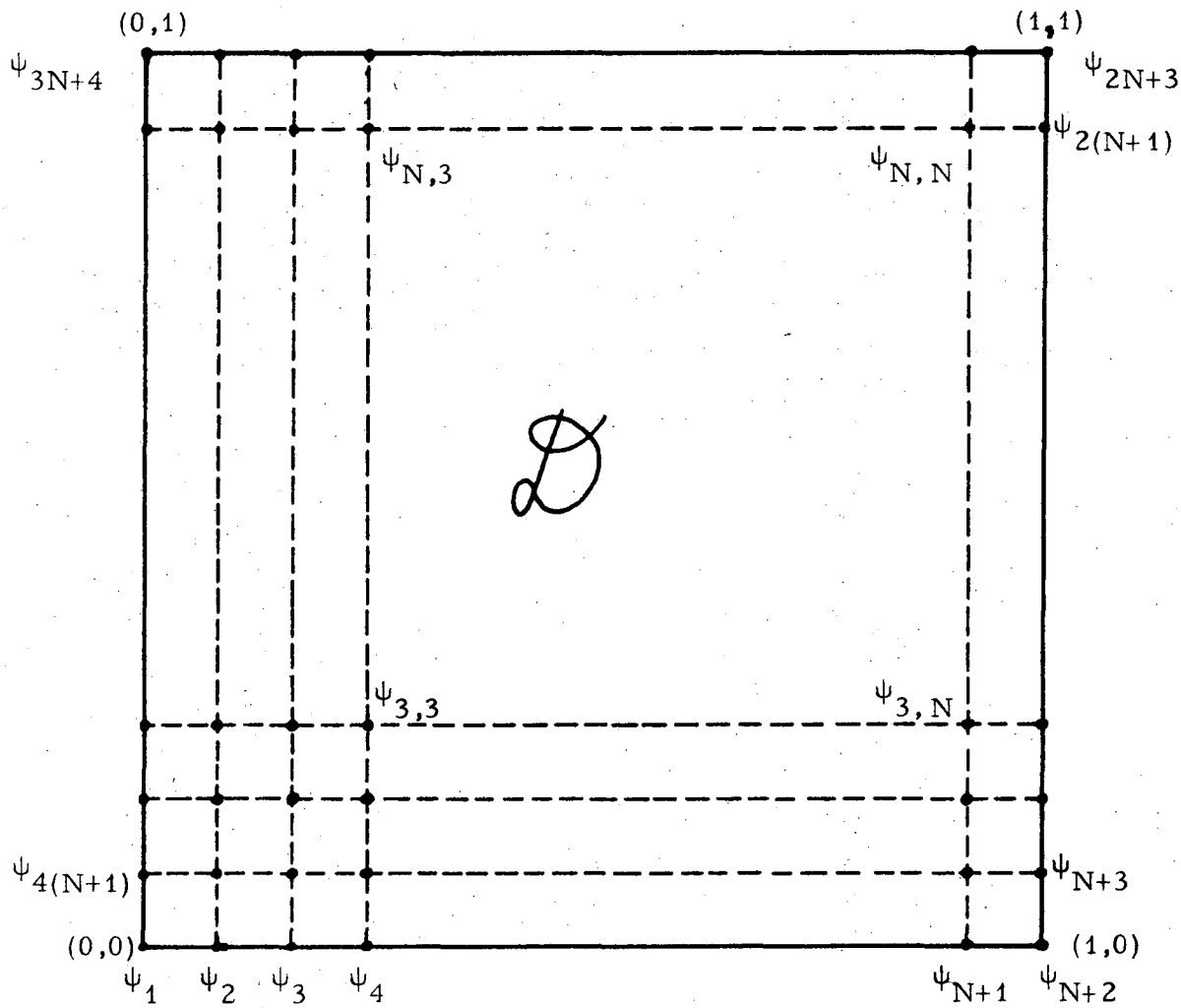

Fig. 5. Location of grid values of potential stream function.

This gives a total of $(N + 2)^2$ function values. As mentioned previously, if it is necessary to evaluate the spline at an interior mesh point, it is necessary to find the "nearest" nine spline coefficients, which are stored over the original function values. A problem arises when the spline needs to be evaluated near a boundary grid point, as, for example, to calculate the vorticity in the boundary layer. In that case, it becomes necessary to know some spline coefficients "falling outside" $\mathcal{D}$ (Fig. 6).

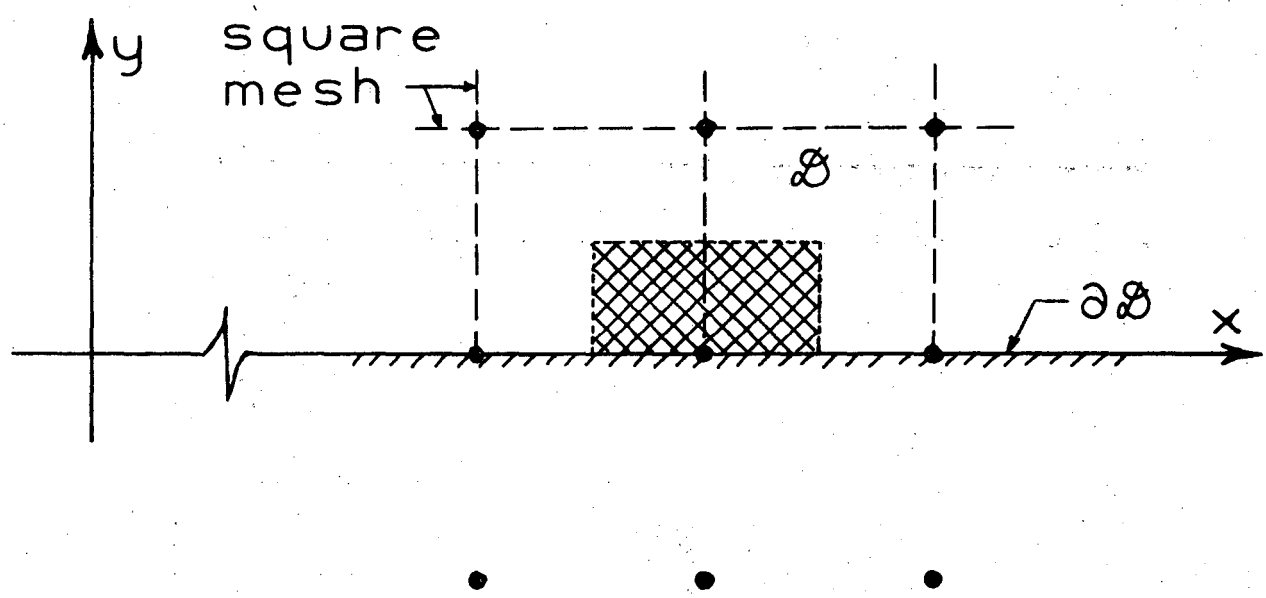

Fig. 6. "Location" of spline coefficients on the boundary y = 0.

The points • falling outside the domain are coefficients which will need to be evaluated if the spline needs to be calculated in the shaded region. A similar problem arises when the spline needs to be evaluated near one of the corners (0,0), (0,1), (1,1), or (1,0). (Fig. 7)

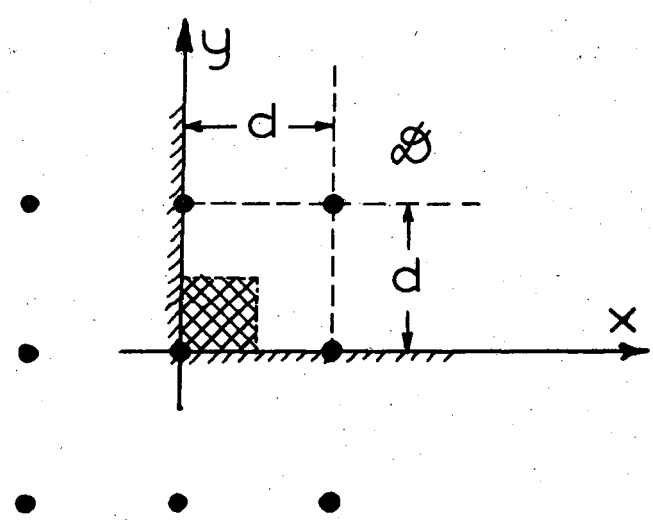

Fig. 7. "Location" of spline coefficients in the corner x = y = 0.

After some arithmetic, it is evident that to be able to evaluate the spline everywhere in $\mathcal{D}$, it is necessary to know a total of $(N + 4)^2$ spline coefficients. For simplicity the spline may be arranged in a table (Fig. 7) over the old grid function values.

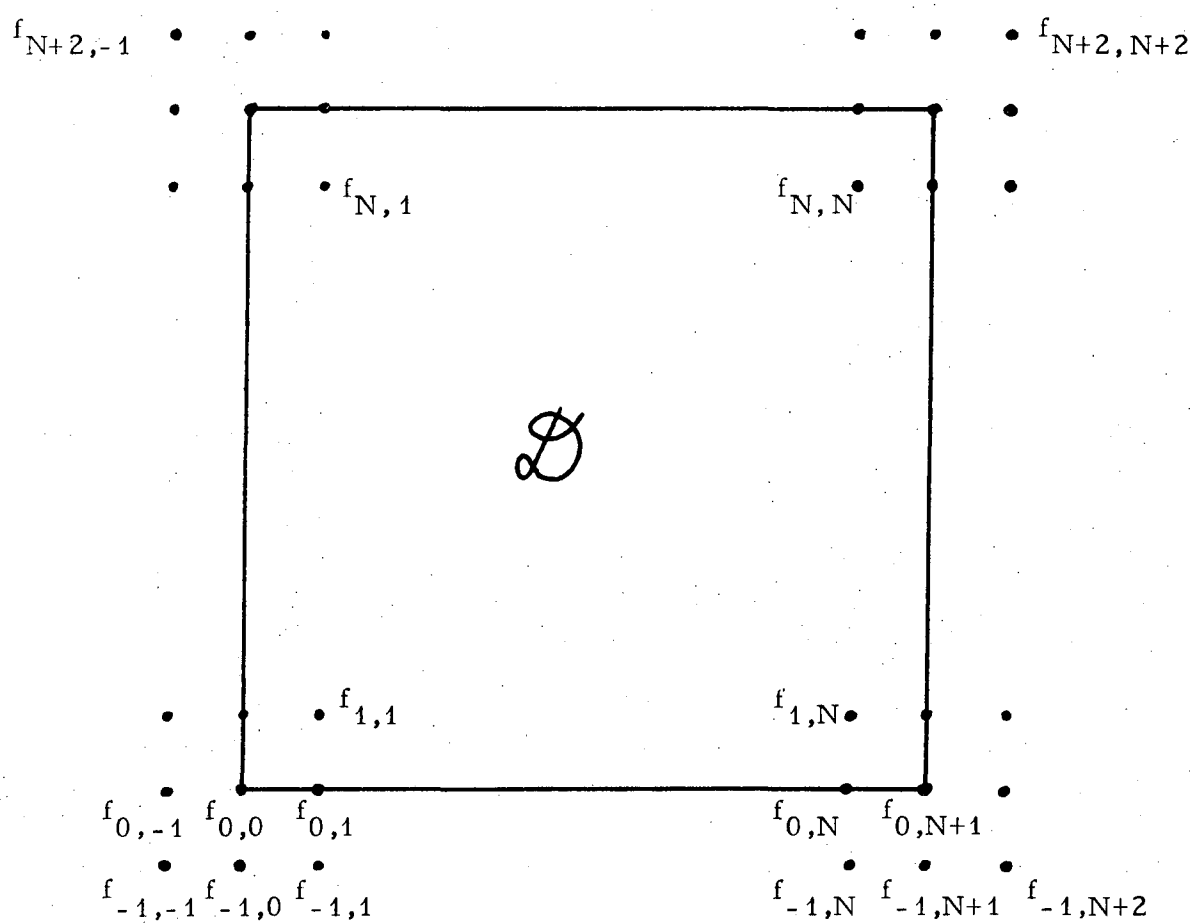

Fig. 8. Arrangement of spline coefficients.

The following section describes the $(N + 4)^2$ linear equations that the spline coefficients must satisfy.

4.3. Linear equations for the spline coefficients

To begin, it is easy to write down $(N + 2)^2$ linear equations by requiring that the spline interpolator agree with the function values at the N^2 interior grid points and the $4(N + 1)$ boundary points. For example, if the spline must be correct at (0,0), then using Eqs. (26) and (27) obtain,

$$\psi(0,0) = g_0^{(0)}(0) + \frac{d^2}{8}\,\delta_{0j}^2 g_j^{(0)}(0)$$

$$= \frac{1}{64}\,[36 f_{0,0} + 6(f_{0,1} + f_{1,0} + f_{-1,0} + f_{-1,0})$$

$$+ f_{1,1} + f_{1,-1} + f_{-1,1} + f_{-1,-1}]$$

or,

$$64\,\psi(0,0)$$

$$= f_{-1,-1} + 6 f_{-1,0} + f_{-1,1} + 6(f_{0,-1} + 6 f_{0,0} + f_{0,1}) + f_{1,-1}$$

$$+ 6 f_{1,0} + f_{1,1}\,.$$

Similar equations will hold at the remaining $(N+2)^2-1$ boundary and interior grid points.

However, $(N+4)^2$ coefficients have been used in the $(N+2)^2$ equations; hence $(N+4)^2 - (N+2)^2 = 4N + 12$ more equations are needed in order to have as many equations as unknowns. After some examination it is evident that the normal derivative of the spline at the boundary can be arbitrarily prescribed. Letting $f = f(x,y)$ denote the spline, it follows that $\frac{\partial f}{\partial n} = \underline{u}_p \cdot \underline{s}$. Since by construction, $\frac{\partial f}{\partial s} = -\underline{u}_p \cdot \underline{n} = \underline{u}_\zeta \cdot \underline{n}$ the spline generates an approximation to a potential flow which nullifies the normal velocity at the boundary, due to the vortices. It is then tempting to prescribe $\frac{\partial f}{\partial n} = -\underline{u}_\zeta \cdot \underline{s}$, and thereby construct a velocity field satisfying both boundary conditions. However, I felt that this would give rise to an unreasonably non-smooth potential flow, hence the temptation was resisted, and $\frac{\partial f}{\partial n}$ was set equal to a backward, second-order correct, divided difference of the function values. Looking at Fig. 9,

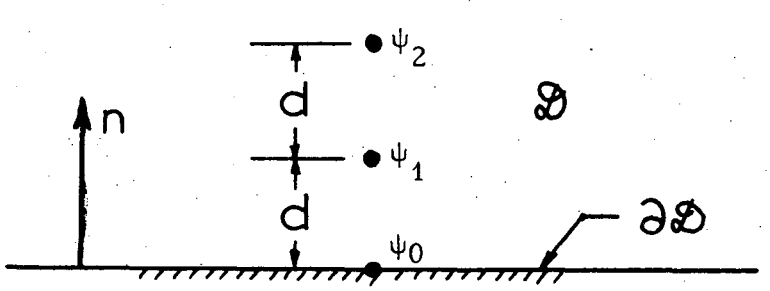

Fig. 9. Three grid function values near a boundary.

Let ψ_i denote the grid function values at the points ● . It is then easy to verify that

$$\frac{1}{d}\left(2\psi_1 - \frac{3}{2}\psi_0 - \frac{1}{2}\psi_2\right) = \frac{\partial\psi}{\partial n} + \mathcal{O}(d^2) .$$

To transform this into an equation for the spline coefficients, assume that we wish to write an equation for the coefficient $f_{-1,j}$ (Fig. 10).

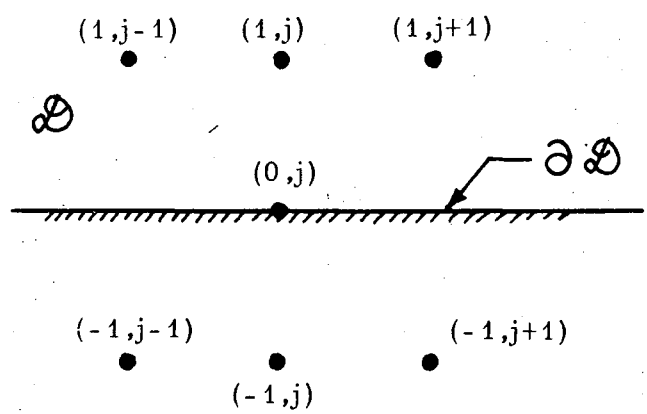

Fig. 10. Numbering of several spline coefficients near the boundary y = 0.

Using Eqs. (26) and (27) evidently

$$\frac{1}{d}\left(2\psi_{1,j} - \frac{3}{2}\psi_{0,j} - \frac{1}{2}\psi_{2,j}\right) = \frac{\partial\psi}{\partial n} = \frac{\partial f}{\partial y}(0,jd)$$

$$= \frac{1}{16d}\left[f_{1,j+1} + f_{1,j-1} - f_{-1,j+1} - f_{-1,j-1} + 6(f_{1,j} - f_{-1,j})\right],$$

or

$$32\psi_{1,j} - 24\psi_{0,j} - 8\psi_{2,j} = -f_{-1,j-1} - 6f_{-1,j} - f_{-1,j+1} + f_{1,j-1} + 6f_{1,j} + f_{1,j+1}.$$

A similar equation holds at the vertical boundaries (Fig. 11)

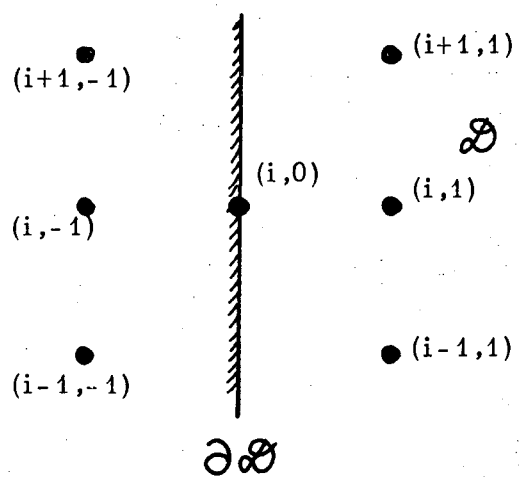

Fig. 11. Numbering of spline coefficients near the boundary x = 0.

i.e.,

$$32\,\psi_{i,1} - 24\,\psi_{i,0} - 8\,\psi_{i,2}$$

$$- f_{i-1,\,-1} + f_{i-1,\,1} - 6 f_{i,\,-1} + 6 f_{i,} \quad - f_{i+1,\,-1} + f_{i+1,\,1}.$$

This gives a total of 4N such equations for the coefficients $f_{-1,j}$, $f_{j,-1}$, $f_{N+2,j}$, $f_{j,N+2}$, for $j = 1, 2, \cdots, N$.

It is now necessary to write down equations for the twelve remaining coefficients, $f_{-1,-1}$, $f_{-1,0}$, $f_{0,-1}$, $f_{-1,N+1}$, $f_{-1,N+2}$, $\cdots$ i.e., the coefficients,

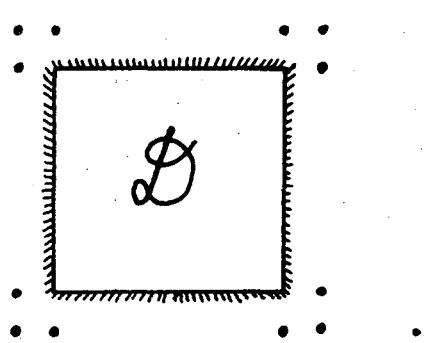

The twelve equations will be derived by prescribing values for the first order derivatives of the spline, $\partial f/\partial x$ and $\partial f/\partial y$, and the second order mixed derivative $\partial^2 f/\partial x \partial y$ at the 4 corners (0,0), (0,1), (1,0) and (1,1). Since f is the approximation to the potential stream function, i.e., $\underline{u}_p = (\partial_y f, -\partial_x f)$, it is allowable to prescribe the velocity $\underline{u} = \underline{u}_p + \underline{u}_\zeta$ to be zero at the corners by writing

$$\underline{u}_p = (\partial_y f, -\partial_x f) = -\underline{u}_\zeta = (-u_\zeta, v_\zeta). \tag{28}$$

Equation (28) transforms into 8 equations for the spline coefficients; in particular at corner 1, $(x,y) = (0,0)$ we get,

$$\frac{\partial f}{\partial x}(0,0) = v_\zeta(0,0) \tag{29}$$

$$\frac{\partial f}{\partial y}(0,0) = -u_\zeta(0,0), \tag{30}$$

or

$$16\, d\, v_\zeta(0,0) = -f_{-1,-1} + f_{-1,1} - 6f_{0,-1} + 6f_{0,1} - f_{1,-1} - f_{1,-1} \tag{29.5}$$

$$-16\, d\, u_\zeta(0,0) = -f_{-1,-1} - 6f_{-1,0} - f_{-1,1} + f_{1,-1} + 6f_{1,0} + f_{1,1}. \tag{30.5}$$

To derive 4 equations for the corner coefficients, $f_{-1,-1}$, $f_{-1,N+2}$, $f_{N+2,N+2}$, $f_{N+2,-1}$ set the second order mixed partial of the spline equal to the backwards, second order correct, divided difference of the computed stream function; that is, labeling the stream function as in Fig. 12:

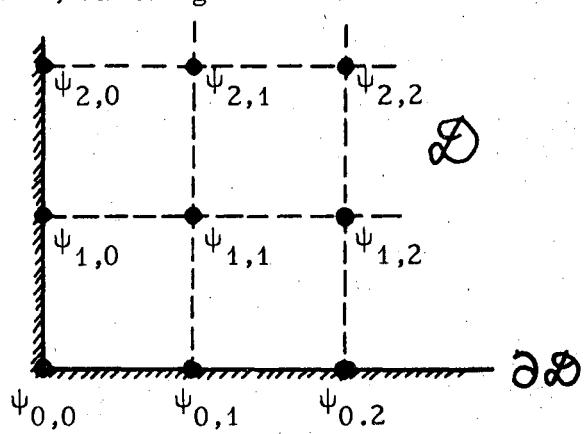

Fig. 12. Labeling of stream function values in the corner $x = y = 0$.

Then,

$$9\psi_{0,0} - 12(\psi_{0,1} + \psi_{1,0}) + 3(\psi_{0,2} + \psi_{2,0}) + 16\psi_{1,1}$$
$$- 4(\psi_{1,2} + \psi_{2,1}) + \psi_{2,2} = 4d^2 \frac{\partial^2\psi}{\partial x \partial y} + \mathcal{O}(d^4), \tag{31}$$

and using (26) and (27)

$$\frac{\partial^2 f}{\partial x \partial y}(0,0) = \frac{1}{4d^2}(f_{-1,-1} - f_{-1,1} - f_{1,-1} + f_{1,1}) . \tag{32}$$

Labeling the left hand side of Eq. (31) C1, at the corner 1, $(x,y) = (0,0)$, we get

$$C1 = f_{-1,-1} - f_{-1,1} - f_{1,-1} + f_{1,1} ,$$

with similar equations at the remaining corners.

4.4. Solution of system for the spline coefficients

This section presents the matrix equation for the spline coefficients and its solution.

Using the last section, define

$$\underline{\underline{f}} \equiv (\underline{f}_{-1}, \underline{f}_0, \underline{f}_1, \cdots, \underline{f}_{N+2})^T$$

where

$$\underline{f}_i \equiv (f_{i,-1}, f_{i,0}, f_{i,1}, \cdots, f_{i,N+2})^T .$$

The equation to solve is

$$M\underline{\underline{f}} = \underline{y} , \tag{33}$$

where $\underline{y} \equiv (\underline{y}_{-1}, \underline{y}_0, \underline{y}_1, \cdots, \underline{y}_{N+2})^T$

and

$$\underline{y}_j = (y_{j,-1}, y_{j,0}, y_{j,1}, \cdots, y_{j,N+2})^T$$

is the vector containing the stream function values at the grid points as well as values of its derivatives at the boundary. The matrix M has the form

$$M = \begin{bmatrix} -A & O & A & & & & \\ A & 6A & A & & & & \\ & A & 6A & A & & & \\ & & A & 6A & A & & \\ & & & \cdot & \cdot & \cdot & \\ & & & & A & 6A & A \\ & & & & -A & O & A \end{bmatrix} ,$$

where,

$$A = \begin{bmatrix} -1 & 0 & 1 & & & & \\ 1 & 6 & 1 & & & & \\ & 1 & 6 & 1 & & & \\ & & \cdot & \cdot & \cdot & & \\ & & & \cdot & \cdot & \cdot & \\ & & & & 1 & 6 & 1 \\ & & & & -1 & 0 & 1 \end{bmatrix}$$

The non-singularity of M is proved by exhibiting its inverse. The method of solution uses the Sherman-Woodbury formula and closely follows a method presented by Widlund [9].

Initially the system Eq.(33) is transformed into the system

$$M_\mu \underline{f} = \underline{y}_\mu \tag{34}$$

where

$$M_\mu = \begin{bmatrix} -A_\mu & 0 & A_\mu & & & & \\ A_\mu & 6A_\mu & A_\mu & & & & \\ & A_\mu & 6A_\mu & A_\mu & & & \\ & & \cdot & \cdot & \cdot & & \\ & & & \cdot & \cdot & \cdot & \\ & & & & A_\mu & 6A_\mu & A_\mu \\ & & & & -A_\mu & 0 & A_\mu \end{bmatrix},$$

$$A_\mu = \begin{bmatrix} \mu & 0 & -\mu & & & & \\ 1 & 6 & 1 & & & & \\ & 1 & 6 & 1 & & & \\ & & \cdot & \cdot & \cdot & & \\ & & & \cdot & \cdot & \cdot & \\ & & & & 1 & 6 & 1 \\ & & & & -1 & 0 & 1 \end{bmatrix},$$

and for $i = -1, 0, 1, 2, \cdots, N+2$

$$(y_\mu)_{i,-1} = -\mu y_{i,-1}$$

$$(y_\mu)_{i,j} = y_{i,j}, \quad \text{for } j \neq -1.$$

In other words, multiply every $(N+4)^{\underline{th}}$ equation by $-\mu$, beginning with the first. μ is a solution of the equation

$$\frac{1}{\mu} + \mu = 6,$$

and the reason for this transformation will become evident shortly.

Assuming for the moment that A_μ^{-1} exists and is easy to obtain, pre-multiply every "matrix row" of Eq. (34) by A_μ^{-1}, obtaining

$$E\underline{\underline{f}} = \underline{\underline{z}} \tag{35}$$

where,

$$E = \begin{bmatrix} -I & O & I & & & & \\ I & 6I & I & & & & \\ & I & 6I & I & & & \\ & & \cdot & \cdot & \cdot & & \\ & & & \cdot & \cdot & \cdot & \\ & & & & I & 6I & I \\ & & & & -I & O & I \end{bmatrix},$$

I is the diagonal matrix,

$$\underline{\underline{z}} \equiv (\underline{z}_{-1}, \underline{z}_0, \underline{z}_1, \cdots, \underline{z}_{N+2})^T,$$

and for $i = -1, 0, 1, \cdots, N+2$,

$$\underline{z}_i \equiv A_\mu^{-1} (\underline{y}_\mu)_i.$$

Equation (35) is then transformed into

$$E_\mu \underline{\underline{f}} = \underline{\underline{z}}_\mu \tag{36}$$

where,

$$E_\mu \equiv \begin{bmatrix} \mu I & O & -\mu I & & & & \\ I & 6I & I & & & & \\ & I & 6I & I & & & \\ & & \cdot & \cdot & \cdot & & \\ & & & \cdot & \cdot & \cdot & \\ & & & & I & 6I & I \\ & & & & -I & O & I \end{bmatrix},$$

and $\underline{\underline{z}}_\mu \equiv (\mu \underline{z}_{-1}, z_0, \underline{z}_1, \cdots, \underline{z}_{N+2})^T$. Equation (36) is now "uncoupled" and can be solved for $\underline{\underline{f}}$ by solving N + 4 systems of the type

$$A_\mu \underline{g}_k = \underline{b}_k \ , \ k = -1, 0, 1, \cdots, N+2,$$

where

$$\underline{b}_k \equiv (-\mu z_{-1,k}, z_{0,k}, z_{1,k}, \cdots, z_{N+2,k})^T.$$

Consider now the evaluation of A_μ^{-1}. The system to solve is

$$A_\mu \underline{x} = \underline{b}$$

where

$$A_\mu = \begin{bmatrix} \mu & O & -\mu & & & & \\ 1 & 6 & 1 & & & & \\ & 1 & 6 & 1 & & & \\ & & \cdot & \cdot & \cdot & & \\ & & & \cdot & \cdot & \cdot & \\ & & & & 1 & 6 & 1 \\ & & & & -1 & O & 1 \end{bmatrix}$$

and $\mu = 3 + \sqrt{8}$ is a solution of $\frac{1}{\mu} + \mu = 6$. Note that, by defining,

$$\underline{u} \equiv (1, 0, 0, \ldots, 0)^T, \quad v \equiv (0, -1, -\mu, 0, 0 \ldots 0)^T,$$

and

$$B \equiv \begin{bmatrix} \mu & 1 & & & & & \\ 1 & 6 & 1 & & & & \\ & 1 & 6 & 1 & & & \\ & & \cdot & \cdot & \cdot & & \\ & & & \cdot & \cdot & \cdot & \\ & & & & 1 & 6 & 1 \\ & & & & -1 & O & 1 \end{bmatrix},$$

then $A_\mu = B + uv^T$. Hence using the Sherman-Woodbury formula,

$$A_\mu^{-1} = B^{-1} - B^{-1}\,\underline{u}\,(1 + \underline{v}^T B^{-1}\underline{u})^{-1}\underline{v}^T B^{-1}$$

and the solution can be written directly,

$$\underline{x} = B^{-1}\underline{b} - B^{-1}\underline{u}\,(1 + \underline{v}^T B^{-1}\underline{u})^{-1}\underline{v}^T B^{-1}\underline{b}. \tag{37}$$

Define the scalar, $\beta \equiv \underline{v}^T B^{-1}\underline{b}$, then from the definition of $\underline{v}$, it is obvious that

$$\beta = -\,[(B^{-1}\underline{b})_2 + \mu(B^{-1}\underline{b})_3] \tag{38}$$

where $(B^{-1}\underline{b})_k$ is the $k^{\underline{th}}$ element of the vector $B^{-1}\underline{b}$. The matrix B has a ready L U decomposition, namely,

$$B = LU \equiv \begin{bmatrix} 1 & & & & & & \\ 1/\mu & 1 & & & & & \\ & 1/\mu & 1 & & & & \\ & & \cdot & \cdot & & & \\ & & & \cdot & \cdot & & \\ & & & & 1/\mu & 1 & \\ & & & & -1/\mu & 1/\mu^2 & 1 \end{bmatrix} \begin{bmatrix} \mu & 1 & & & & & \\ & \mu & 1 & & & & \\ & & \mu & 1 & & & \\ & & & \cdot & \cdot & & \\ & & & & \cdot & \cdot & \\ & & & & & \mu & 1 \\ & & & & & & 1 - 1/\mu^2 \end{bmatrix}$$

and it is now evident that it is necessary that $\frac{1}{\mu} + \mu = 6$, or for stability,

$$\mu = 3 + \sqrt{8}\ .$$

The evaluation of $B^{-1}\underline{b}$ for the first term of Eq. 37 is now trivial since B has been decomposed into a product of triangular matrices; while the evaluation of $B^{-1}\underline{u}$ can be done analytically by induction. To solve the system

$$B\underline{y} = \underline{u},$$

where $\underline{y} = (y_1, \cdots, y_N)^T$, $\underline{u} = (u_1, \cdots, u_N)^T$,

first solve the system,

$$L\underline{z} = \underline{u}, \text{ getting}$$

$z = (z_1, z_2, \cdots, z_N)^T$ where for $j = 1, 2, \cdots, N-1$,

$z_j = (-1/\mu)^{j-1}$ and $z_N = (-1/\mu)^{N-2}(1 + 1/\mu^2)$;

Then solve the system,

$$U\underline{y} = \underline{z}$$

getting,

$$y_N = (-1/\mu)^{N+2} \left(\frac{1 + \mu^2}{1 - \mu^2} \right) ,$$

$$y_{N-1} = (-\frac{1}{\mu})^{N-3} \frac{2}{1 - \mu^2} ,$$

and

$$y_j = (-\frac{1}{\mu})^{2N-j-4} \left(\frac{1 + \mu^{2(N-j-1)}}{1 - \mu^2} \right) ,$$

for $j = 1, 2, \cdots, N-2$.

It is then easy to verify that

$$v^T B^{-1} u = -(1/\mu^2)^{N-3} ,$$

hence

$$(1 + v^T B^{-1} u) = [1-(1/\mu^2)^{N-3}]^{-1}$$

and since $\mu^2 \approx 33.92$, make the simplification that,

$$(1 - (1/\mu^2)^{N-3})^{-1} = 1;$$

this is valid since N-3 will be a large integer (> 20). Therefore,

$$B^{-1}\underline{u}(1 + \underline{v}^T B^{-1}\underline{u})^{-1}\underline{v}^T B^{-1}\underline{b} = \beta B^{-1}\underline{u}$$

where β has been evaluated previously by Eq. (38). The computation of $\beta B^{-1}\underline{u}$ proceeds inductively as follows: define

$$c \equiv \beta/(1-\mu^2),$$

$$a_1 \equiv c\,(-1/\mu)^{2N-5} , \quad \text{and} \quad b_1 \equiv \mu^{2(N-2)}$$

and if $\underline{z} \equiv \beta B^{-1}\underline{u}$, it follows that

$z_1 = a_1(1 + b_1)$, while for

$j = 2, 3, \cdots, N$, letting

$$a_j \equiv -\mu a_{j-1}, \qquad b_j = b_{j-1}/\mu^2,$$

get

$$z_j = a_j(1 + b_j).$$

Thence, using the evaluated vector $\underline{z}$, we have, from Eq. (37), that the solution

$$\underline{x} = A_\mu^{-1}\underline{b} = B^{-1}\underline{b}-\underline{z}$$

Q.E.D.

This concludes the calculation of the potential flow.

4.5. Timing tests for the potential flow calculation

The calculation of the spline coefficients $f_{i,j}$ involves solving two large linear systems of equations, but, using modern techniques, these solutions can be obtained relatively inexpensively on large computers.

The first large system to solve is

$$F\underline{\Psi} = \underline{y}$$

where $\underline{\Psi}$ is the array of the grid function values of the potential stream function. The numerical program used a mesh size of

$$d = 1/64,$$

and hence, there were 63^2 unknown interior grid function values. Using the cyclic odd-even reduction algorithm [6], I wrote a routine which, when tested against the test function $\psi = e^x \cos y$ on the unit square, obtained the result in .1 sec with a maximum error of 10^{-6}.

The second large system is Eq. (33), for the array $f_{i,j}$ of the spline coefficients. There are a total of 67^2 spline coefficients, and a test program was run to evaluate the spline coefficients given the grid values of the function $e^x \cos y$ on the unit square. The routine took 6.1×10^{-2} seconds to solve for the coefficients and achieved an accuracy of 10^{-14} when the spline was evaluated at the grid points.

Both test programs were run on the LBL CDC 7600 machine and the timing was done with the library routine SECOND.

5. Numerical Experiment and Results

As described in Section 2, the numerical experiment involved computing the steady-state solution of the two-dimensional flow inside a square cavity induced by one edge sliding in its own plane (Fig. 1).

The program was run for the following sets of parameters:

R = Reynolds number = 10^3,
k = time step = 0.2,
h = boundary discretization length = 1/20,
d = mesh size for potential flow calculation = 1/64,

and initially ($t = 0$) no vorticity was present in the domain $\mathcal{D}$. My hope was to achieve a steady-state distribution of velocity beginning with the fluid at rest.

All of the pictorial output in this report will take the form of Fig. 16 where the boundaries of the square coincide with the outside arrows. Each arrow depicts the magnitude and direction of the velocity at the tail of the arrow. However, due to the relatively large range of the magnitude of the velocity field, $|\underline{u}|$, the lengths of the arrows vary as the square root of $|\underline{u}|$; i.e., if one arrow is half as long as another, the velocity there is 1/4 as small as the velocity of the larger one. Furthermore, the lengths of the arrows are scaled so that the largest occurring velocity draws an arrow as long as the plot mesh size. Note that in Fig. 16, the lower edge has the longest arrows, depicting the velocity at the sliding edge.

Unfortunately, due to the random walk component of the displacement of each vortex, the velocity field, at any one time step, is a random variable, (Fig. 20), and bears little resemblance to the expected velocity distribution. Hence, it was necessary to average many such velocity fields and hope that, by averaging, the random oscillations may be smoothed out. Another question remained unresolved: namely, when to consider that a steady-state had been reached and begin the averaging process. The program has one variable, NCT, that changes drastically at the beginning, namely, the number of vortices present in the fluid. NCT exhibited an almost monotomic growth for the first 100 time steps when it reached 536. After the first 100 time steps, NCT did not exhibit further growth but merely oscillated from one time step to another; in fact, after 420 time steps there were still 547 vortices in the fluid. The averaging process was done over 320 time steps, from the $101^{\underline{st}}$ time step to the $420^{\underline{th}}$, and during this period, the number of vortices varied between 500 and 580. Furthermore, velocity plots were outputted frequently at the

beginning (t = 0), and it was possible to trace the path of the strong vortices as they were shed from the sliding edge, carried downstream, and around the cavity, until, finally by the $100^{\underline{th}}$ time step, there were strong vortices distributed throughout the entire cavity.

The final results are in the form of the average velocity field computed by evaluating $\underline{u} = \underline{u}_p + \underline{u}_\zeta$ at the grid points of the plot. Figure 13 shows velocity field after it has been averaged over the 40 time steps, 381-420. Figure 14 is the velocity averaged over 80 time steps, 341-420. Figure 15 is the velocity averaged over 160 time steps, 261-420, and finally Fig. 16 is the velocity averaged over 320 time steps, (101-420). With each subsequent plot, one can see the random oscillations being smoothed out. The vortex center of Fig. 16 appears to be near the point (x, y) = (.59, .39).

Other data computed in Fig. 17, the velocity induced by the average of $\underline{u}$ at the plot boundary points (which lie on $\partial\mathcal{D}$), and Figs. 18 and 19 depict the plot of the velocity u and v along a horizontal and vertical line through the vortex center.

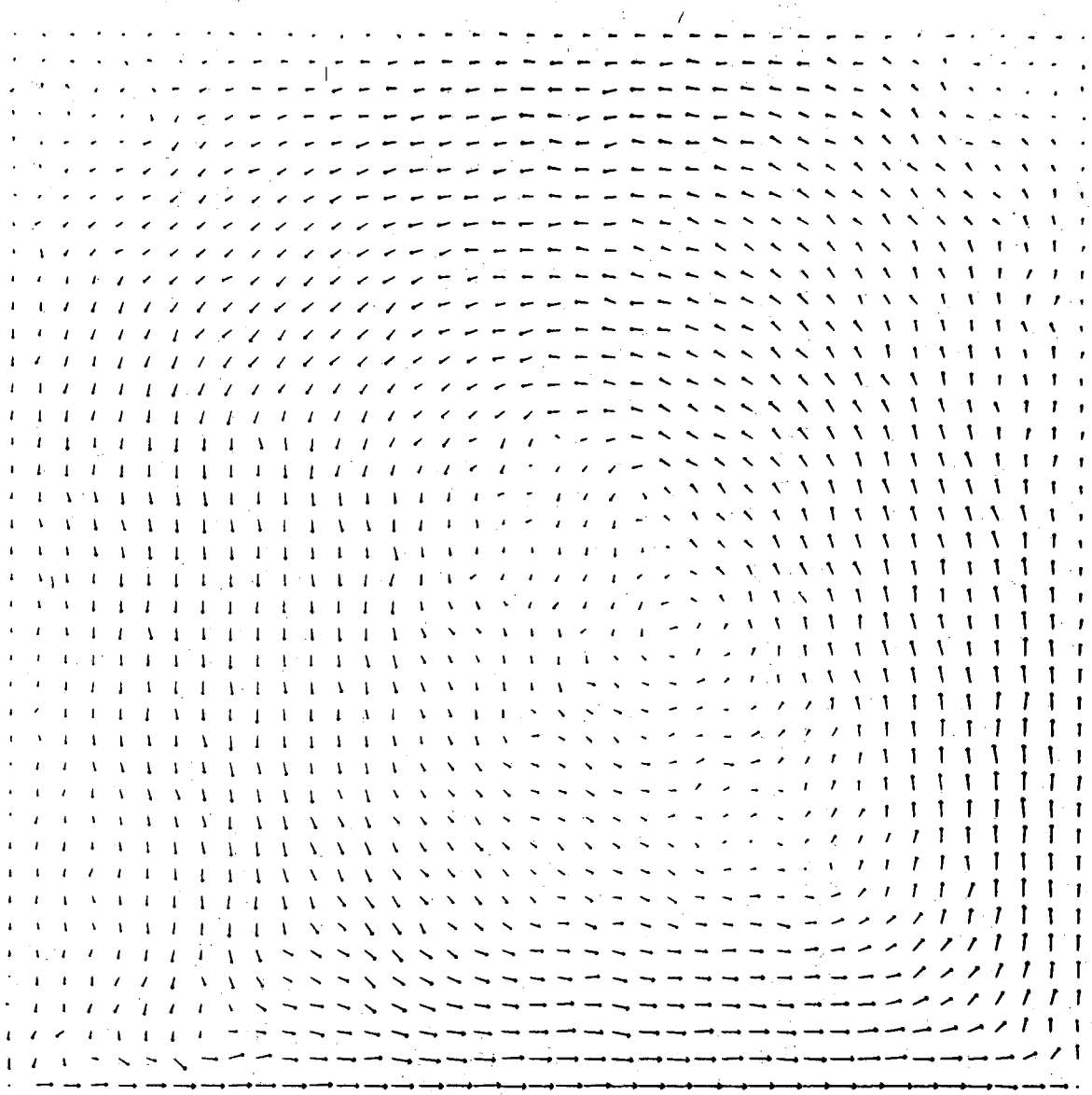

Fig. 13. Average velocity field over the last 40 time steps, 381-420.

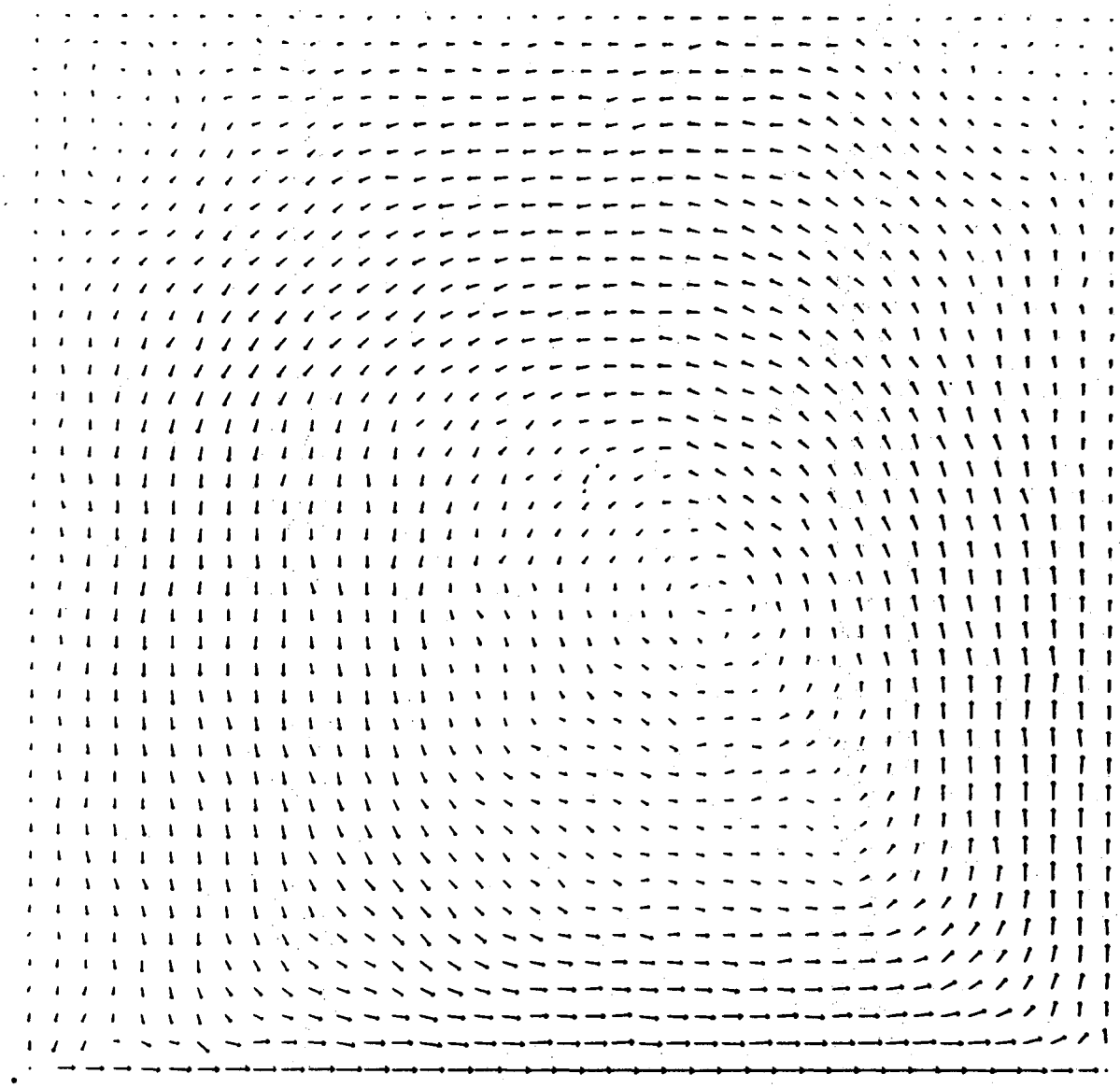

Fig. 14 Average velocity field over the last 80 time steps, 341-420.

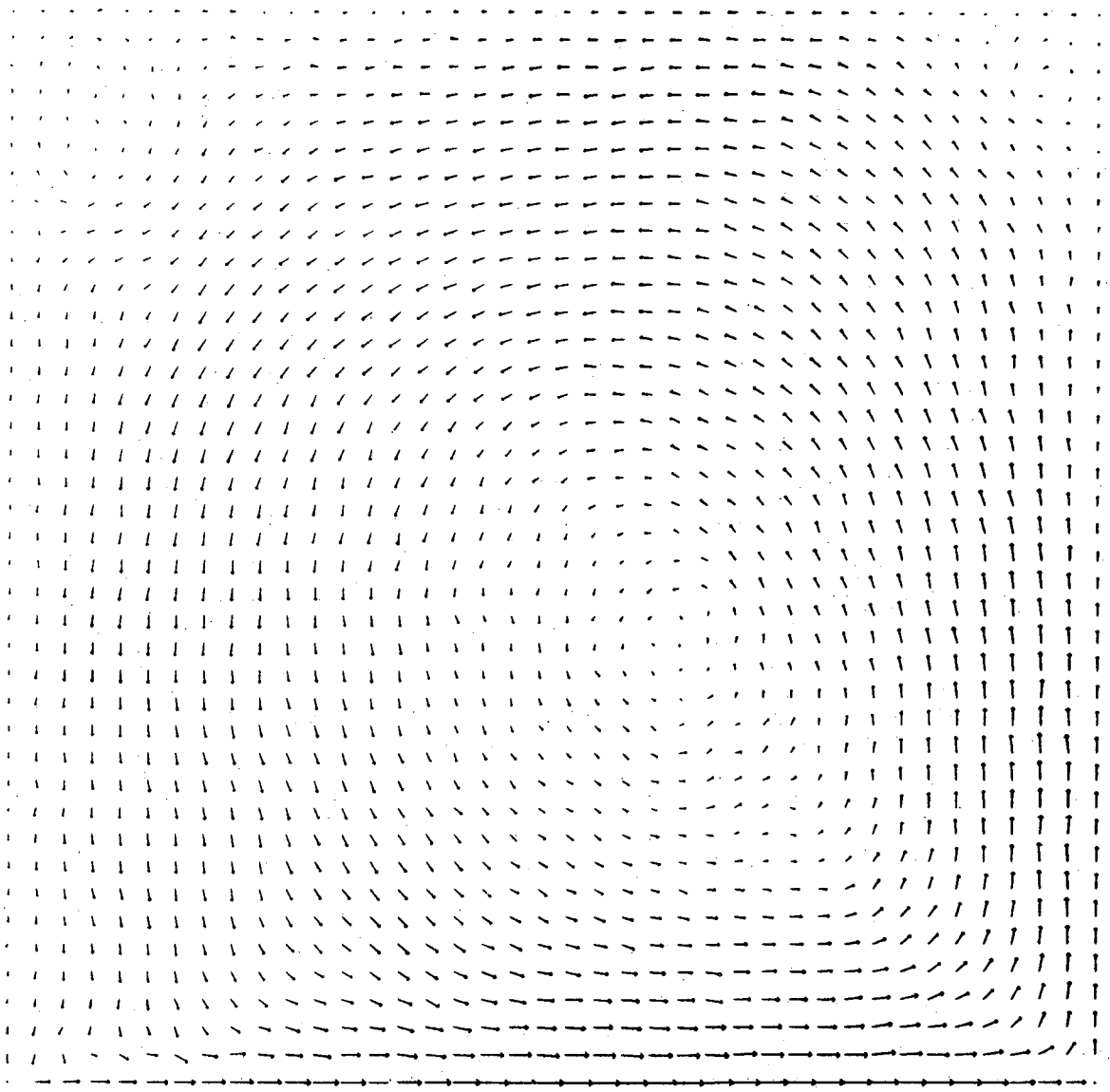

Fig. 15. Average velocity field after the last 160 time steps, 261-420.

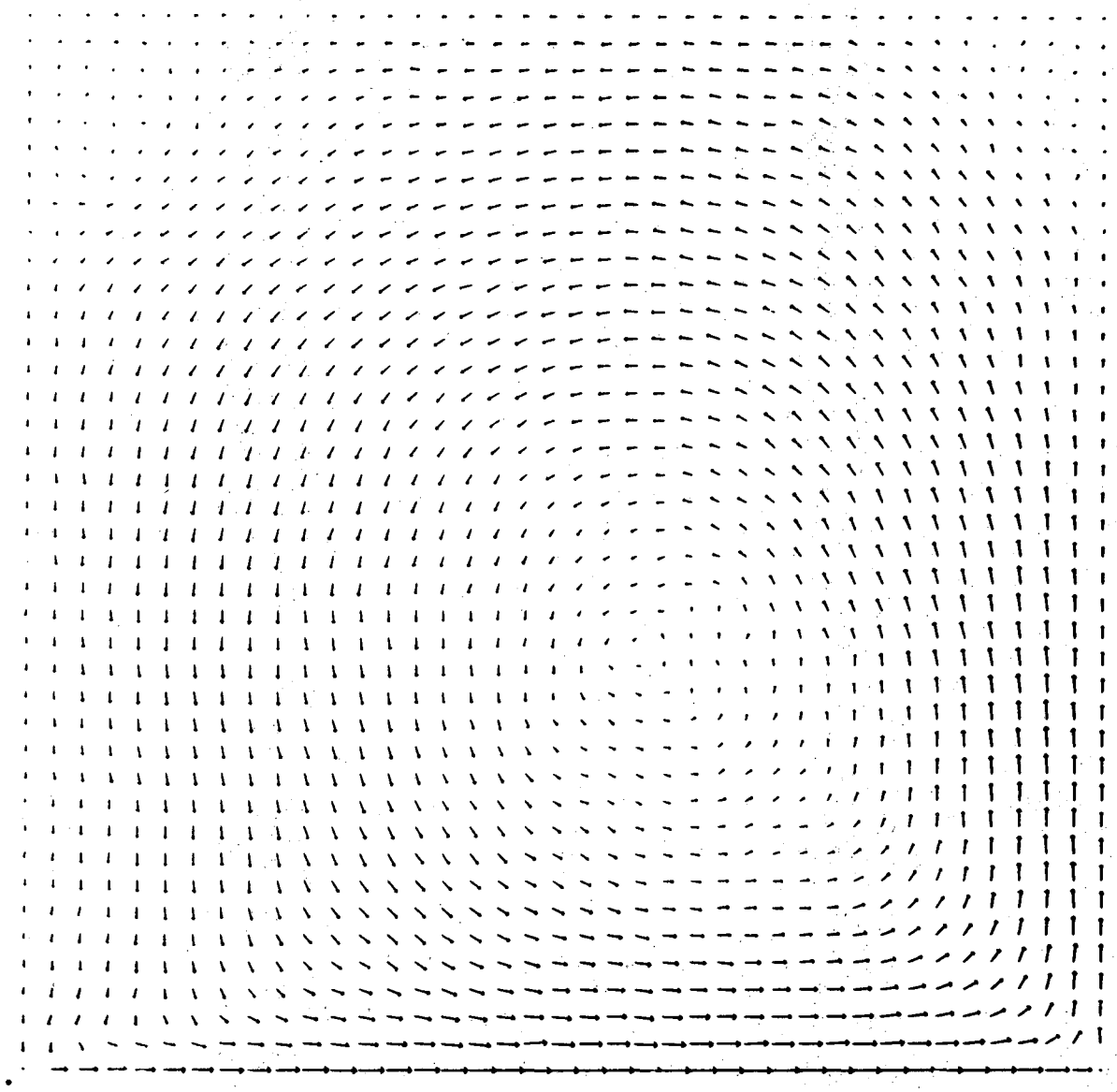

Fig. 16. Average velocity field after the last 320 time steps - 101-420. vortex center ≈ (.59, .39)

Fig. 17. Read velocities traversing the boundary keeping domain $\mathscr{D}$ on your left.

1VELOCITIES ALONG THE BDRY.

K	SIDE 1 U	SIDE 1 V	SIDE 2 U	SIDE 2 V	SIDE 3 U	SIDE 3 V	SIDE 4 U	SIDE 4 V
1	0.	0.	0.	0.	0.	0.	0.	0.
2	0.236066	0.002858	-0.010249	0.255553	0.011469	-0.000429	-0.000438	0.005972
3	0.313567	0.009060	-0.003745	0.257163	0.009378	-0.000291	-0.000158	0.007578
4	0.360064	0.000586	-0.001028	0.255775	0.010371	0.000279	0.000114	0.017381
5	0.367890	-0.002913	0.000867	0.305923	0.005824	0.000267	0.000883	0.019274
6	0.469382	-0.006202	-0.007534	0.290101	0.012787	-0.001027	-0.001771	0.015414
7	0.448378	-0.006415	-0.002627	0.291951	-0.012080	-0.000187	-0.001704	0.014747
8	0.528655	-0.002506	-0.002918	0.266103	-0.009934	0.000048	0.000685	0.013376
9	0.529802	0.007135	0.003213	0.257460	-0.021450	0.001776	0.003572	-0.002252
10	0.553263	0.007369	0.002254	0.230006	-0.033808	0.001410	0.000325	-0.009408
11	0.601020	0.003283	0.001557	0.245223	-0.045790	-0.000307	-0.000219	-0.022880
12	0.597273	-0.002779	0.002883	0.247411	-0.045099	-0.001021	-0.000545	-0.037077
13	0.589646	0.002109	-0.004345	0.244854	-0.040157	0.002318	-0.000445	-0.035955
14	0.593042	0.000040	0.000202	0.202467	-0.052913	0.001144	-0.000085	-0.035240
15	0.611942	-0.005268	0.001708	0.184010	-0.056284	0.002147	-0.003095	-0.043549
16	0.646216	0.000511	-0.000522	0.176108	-0.061903	0.000930	-0.001404	-0.038397
17	0.684083	-0.001011	0.000489	0.147630	-0.064455	0.000287	0.000295	-0.049513
18	0.715859	0.007510	0.000254	0.145647	-0.046925	0.000175	-0.000623	-0.042853
19	0.708535	-0.003797	0.000605	0.119471	-0.039080	-0.001098	-0.001534	-0.040719
20	0.686090	-0.001183	0.000295	0.105163	-0.039245	0.001848	-0.002420	-0.044612
21	0.724567	0.003584	-0.001647	0.107936	-0.043800	0.002708	-0.001728	-0.037718
22	0.715077	0.002640	0.001243	0.096272	-0.033649	-0.000348	0.000168	-0.042564
23	0.725420	0.000191	-0.002339	0.098964	-0.032735	0.001269	-0.003611	-0.027092
24	0.753769	-0.007776	0.001062	0.083061	-0.020514	-0.000631	0.000864	-0.036773
25	0.739526	0.003353	0.000734	0.081040	-0.021995	-0.000770	-0.000899	-0.033049
26	0.738990	0.001240	-0.002625	0.068797	-0.006575	0.000017	0.000020	-0.032572
27	0.735661	0.000863	-0.002502	0.066391	-0.014398	-0.000012	-0.000729	-0.029415
28	0.752624	0.001126	0.003111	0.052446	-0.013984	-0.003840	-0.000352	-0.028346
29	0.753332	0.003750	-0.002778	0.039652	-0.015345	0.000626	-0.000319	-0.029679
30	0.750268	-0.000624	-0.000423	0.020013	-0.003732	-0.000308	-0.000453	-0.010089
31	0.733547	0.004140	-0.000666	0.023998	-0.000545	-0.001008	0.001377	-0.012866
32	0.710856	0.003990	0.001550	0.005983	-0.010574	-0.000851	-0.002420	-0.015763
33	0.696600	0.003143	-0.000457	0.010001	-0.008336	0.000688	-0.002017	-0.027628
34	0.684596	-0.004540	0.001413	0.012235	-0.009604	0.000094	-0.000959	-0.022985
35	0.680802	-0.005594	0.001371	0.000509	-0.004656	0.000490	-0.003076	-0.021566
36	0.623197	0.001005	0.001492	-0.009810	0.002605	0.000386	-0.000583	-0.030110
37	0.563941	-0.003272	0.003357	-0.005493	0.009208	0.001449	-0.004029	-0.031179
38	0.532511	0.004514	-0.000833	-0.007755	0.007947	0.000991	-0.000550	-0.065215
39	0.332809	-0.000739	-0.001764	-0.006099	0.003050	-0.000320	-0.000192	-0.086209

AVERAGE VELOCITIES

SIDE 1 UAV	SIDE 1 VAV	SIDE 2 UAV	SIDE 2 VAV	SIDE 3 UAV	SIDE 3 VAV	SIDE 4 UAV	SIDE 4 VAV
0.594586	0.000497	-0.000496	0.127337	-0.018896	0.000228	-0.000719	-0.023834

SIDE 1: Y = 0 SIDE 2: X = 1 SIDE 3: Y = 1 SIDE 4: X = 0

U ≡ (U,V)

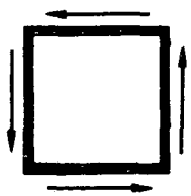

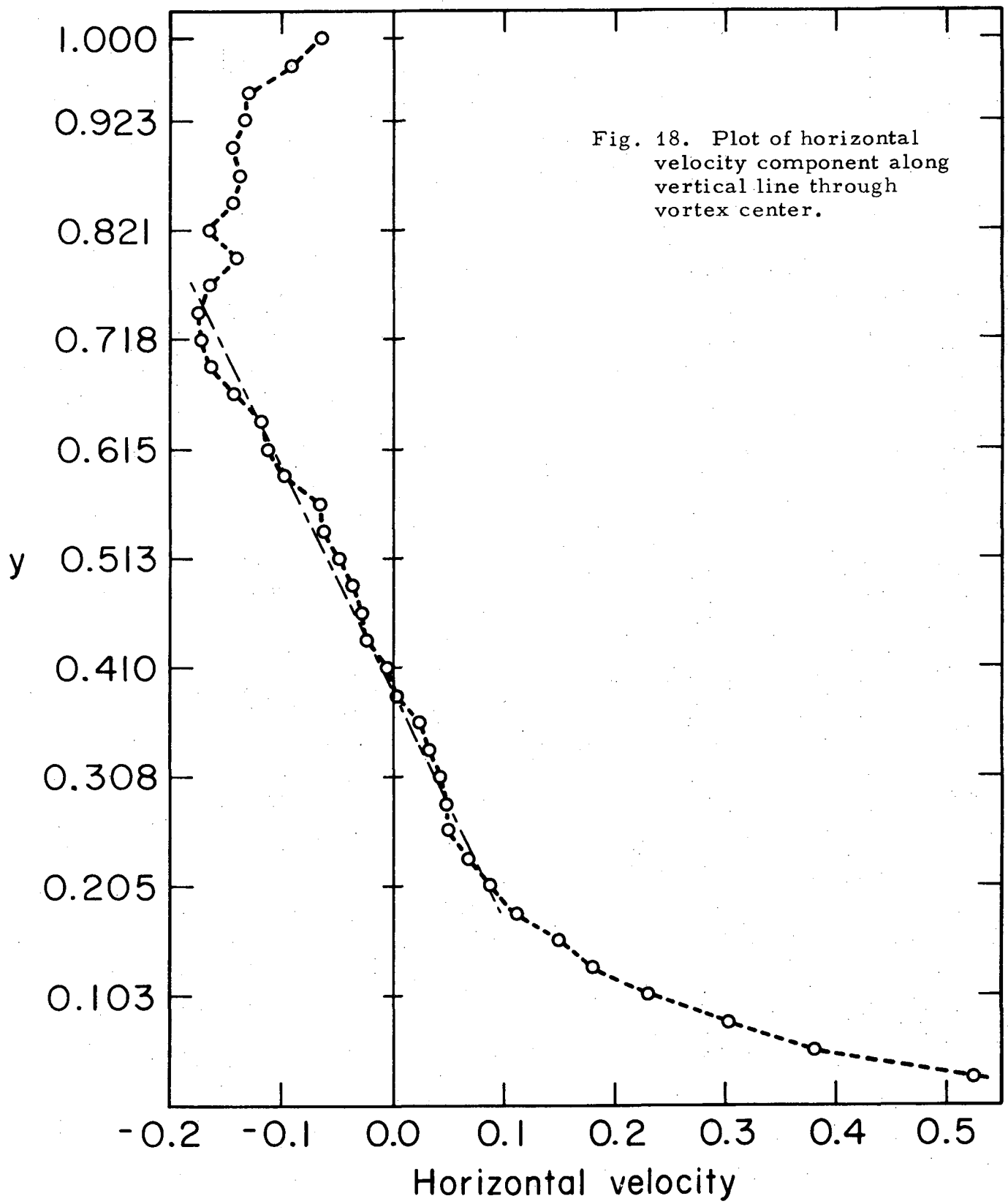

Fig. 18. Plot of horizontal velocity component along vertical line through vortex center.

XBL7412-8372

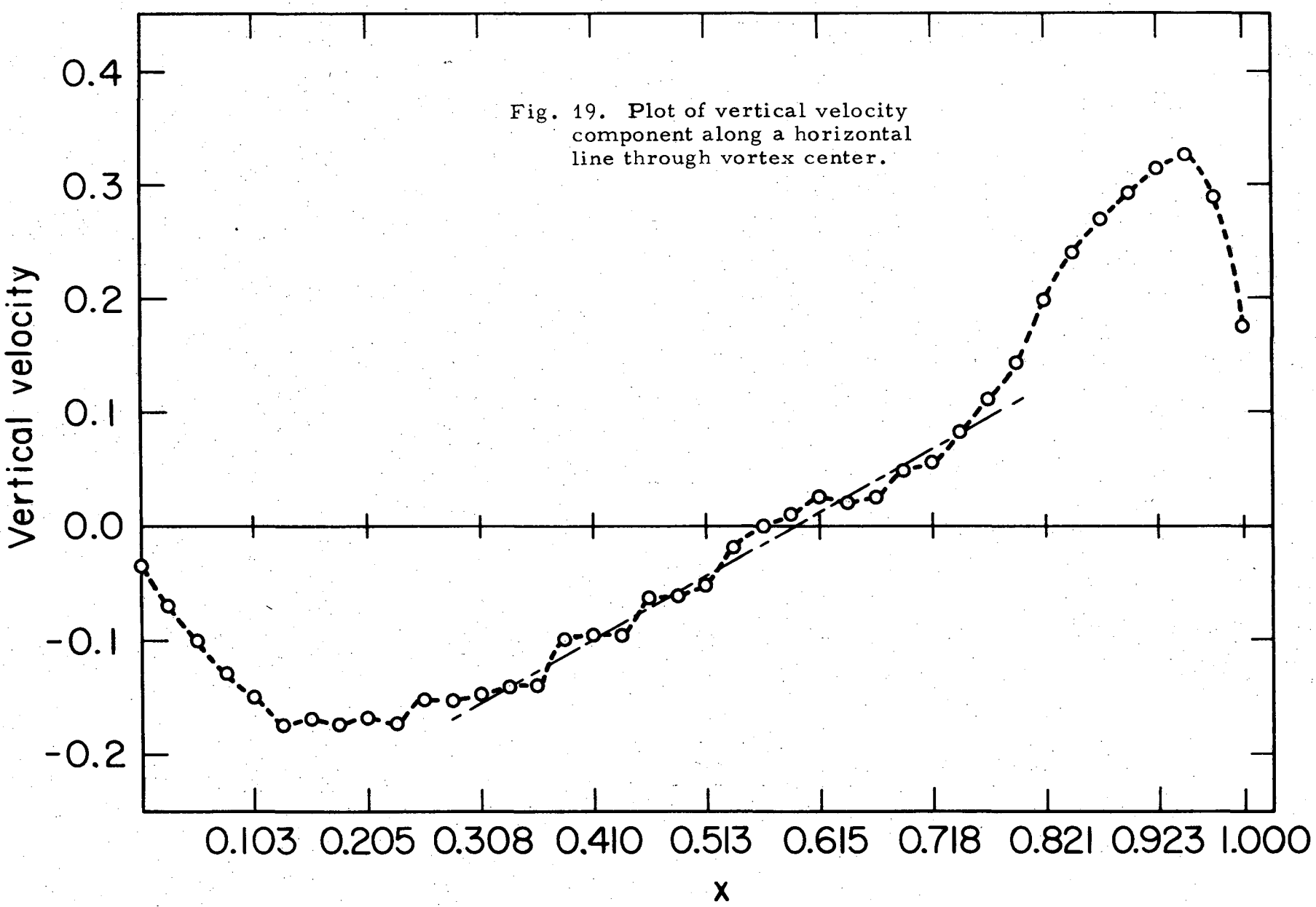

Fig. 19. Plot of vertical velocity component along a horizontal line through vortex center.

XBL7412-8371

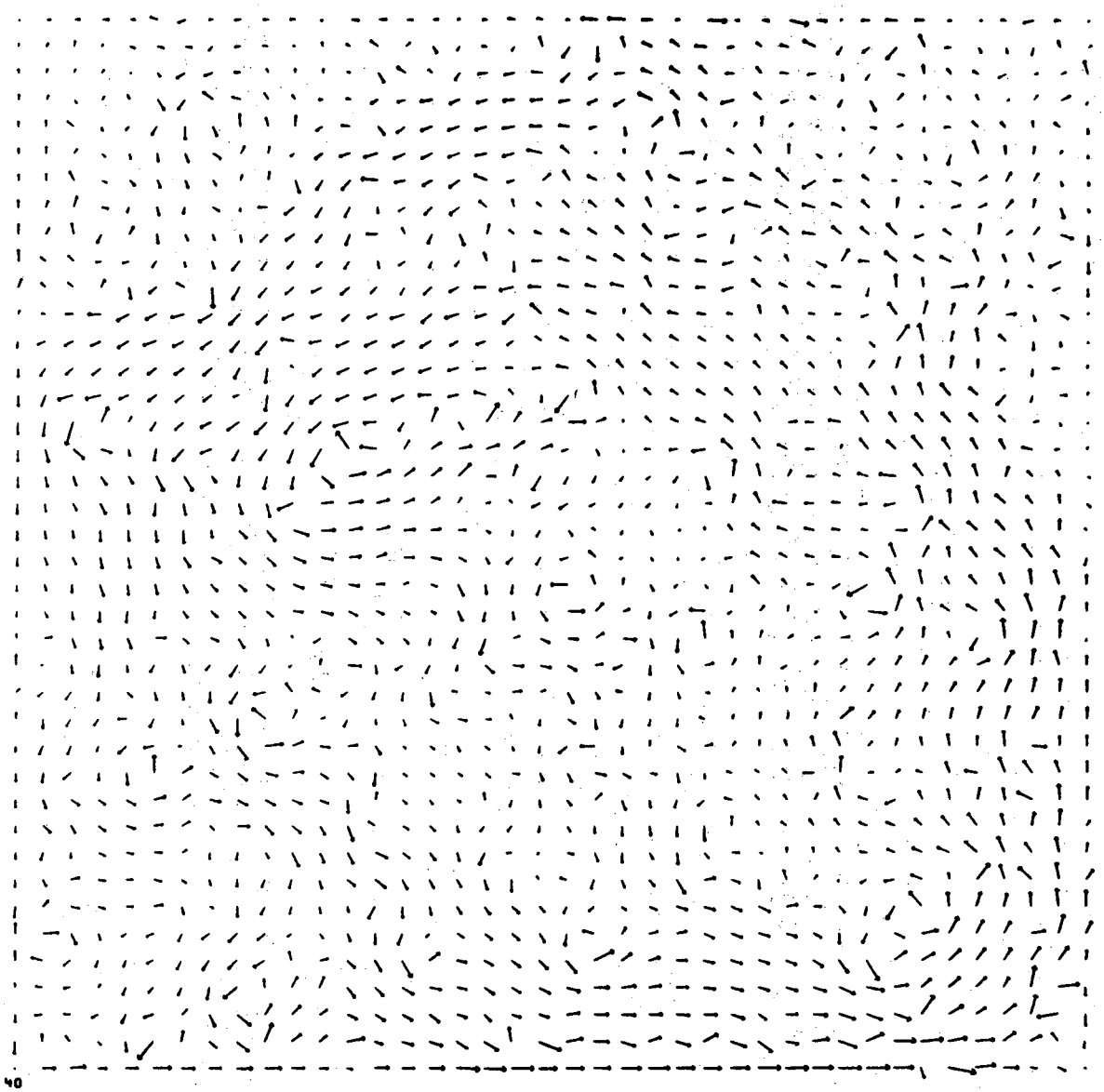

Fig. 20. Typical velocity field, $\underline{u}_p + \underline{u}_\zeta$, at one time step.

6. Discussion of Results

Qualitatively, the results in this report are similar to those predicted by analysis and similar to the numerical results of Bozeman and Dalton [3].

First of all, there does appear to be a large vortex centered slightly downstream and closer to the sliding edge, yet whose strength is felt throughout the cavity. By examining Figs. 18 and 19, it does seem as if there is an inner core of inviscid flow around the vortex center, since the line is almost straight there. Furthermore, there are two counter-rotating vortices in the stationary corners. Note, as well, the peculiar jog that the velocity field exhibits near the leading edge of $y = 0$. This also appears in Bozeman's paper.

However, there are some differences between the results here and those of Bozeman. First the down-stream corner vortex seems to be slightly larger than the upstream vortex, but both, although quite weak do appear on the plots (Fig. 15). Second, the slope of plots 18 and 19 is approximately 0.5 while Bozeman's results seem to have the slope closer to 0.7. This last discrepancy seems to indicate the presence of more vorticity in the center in Bozeman's results. Third, the center of the large vortex does not coincide with Bozeman's center, but rather seems to fall back to where Bozeman places the center for the case $R = 400$.

7. Discussion of Program - Conclusion

Since the vortex method is still in its infancy, much remains to be examined about it.

There is, first of all, no known required relationship between k, the time step, and h, the boundary discretization length, as is often required for stability in finite difference schemes. By examining Figs. 16 and 17, it is evident that the velocity field does not satisfy the tangential boundary condition very well. Mechanically, however, the tangential condition is satisfied by virtue of the creation of a viscous boundary layer. This layer is omnipresent, but the vorticity there has only a local effect at the time of its creation, and its global effect on $\underline{u}$ occurs only after it has diffused into $\mathcal{D}$. It may then, perhaps, be too demanding to require that $\underline{u} \cdot \underline{s}$ be exactly zero, since the vorticity necessary to do exactly that appears in the evaluation of $\underline{u}$ only at the subsequent time step after having diffused from the boundary. Furthermore, I conjecture that better values than those of Fig. 17 could have been attained by either choosing k smaller, or h larger.

Since the standard deviation of the random push for each vortex is $\sqrt{2k/R}$ and the cut-off length $\sigma = h/2\pi$, the choice of parameters (p.27) will cause most of the vortices to travel beyond the cut-off length as they diffuse from the boundary. This does not allow the vortex to cancel completely the tangential velocity component, $\underline{u} \cdot \underline{s}$, hence the poor satisfaction depicted by Figs. 16 and 17. It then seems reasonable to choose k and h such that

$$\alpha \sqrt{\frac{2k}{R}} = \frac{h}{2\pi}$$

where α is some number like 2 or 3; this, I believe, should give a better satisfaction of the boundary conditions.

Some runs were made experimenting with different values for k, and I noticed that by decreasing k, the number of vortices in $\mathcal{D}$ was increased. For example, using the ζ-field after 100 time steps as an input vorticity field, and letting $k = 0.01$ which gives a value of $\alpha \cong 2.5$ above, the number of vortices grew to 820 after only 25 time steps when the program was terminated since there was no more room available to keep track of the vortices. On the other hand, using $k = 0.4$, the number of vortices decreased to a seemingly stable figure at around 320.

It is, however, not very wise to make k too small since the deterministic component of the velocity is $\mathcal{O}(k)$ while the random component is $\mathcal{O}(k^{1/2})$. Hence, if k gets too small, the random component will begin to dominate making the flow look haphazard.

The discrepancy between the slopes of the lines of Figs. 18 and 19 and the results of Bozeman also merit some discussion. As previously noted, the results here seem to indicate the presence of less vorticity than that occurring in Bozeman's experiment. Perhaps, the scheme presented here does not generate enough vorticity at the boundary, and this may be improved by a better approximation to the integral (16); or perhaps, the results of Bozeman display the existence of an artificial grid viscosity greater than the viscosity of the problem of interest. Many such questions still remain unresolved and they certainly merit further study.

Another problem of interest is how one might speed up the calculations. Most of the execution time is spent on computing vortex interactions, since, given N vortices, one must compute N^2 interactions to move them all, and if N is large this becomes costly. In particular, the runs for this problem took an average of 50 seconds per time step on the LLL CDC 6600 'L' machine.

In conclusion, the vortex method seems to give good results for this problem, and it is hoped that it will be tested on other problems, since it may be possible to apply this scheme to problems inaccessible to finite difference methods.

8. References

1. A. Acrivos and F. Pan, "Steady flows in rectangular cavities". J. Fluid Mech. 28 (1967), 643-655.

2. Batchelor, G. K., "On steady laminar flow with closed streamlines at large Reynolds numbers", J. Fluid Mech., 1 (1956), 177-190.

3. J. D. Bozeman and C. Dalton, "Numerical study of viscous flow in a cavity", J. Comp. Phys. 12, (1973) 348-363.

4. O. Buneman, "Subgrid resolution of flow and force fields", J. Comp. Phys., 11 (1973), 250-268.

5. O. Burgraff, "Analytical and numerical studies of the structure of steady separated flows," J. Fluid Mech., 24, (1966), 113-151.

6. B. L. Buzbee, G. H. Golub, and C. W. Nielson, "On direct methods for solving Poisson's equations", SIAM J. Numer. Anal., 7, No. 4, Dec. 1970, 627-656.

7. A. J. Chorin, "Numerical study of slightly viscous flow", J. Fluid Mech., 57, (1973), 785-796.

8. R. Courant, K. O. Friedricks, and H. Dewy, Mathematische Annalen, 100, (1928).

9. D. Fischer, G. Golub, O. Hald, C. Leiva, and O. Widlund, "On Fourier-Toepliz methods for separable elliptic problems, STAN-CS-73-375, July 1973.

10. D. Greenspan, "Numerical studies of prototype cavity flow problems", Comput. J. 12 (1967), 643-655.

11. Kawaguti, M., "Numerical solution of the Navier-Stokes equations for the flow in a two-dimensional cavity", J. Phys. Soc. Japan, 16 (1961), 2307-2315.

12. A. K. Runchal, D. B. Spalding, and M. Wolfshtein "Numerical solution for the elliptic equations for transport of vorticity heat and matter in two-dimensional flow", Phys. Fluid 12 (1969), II-21-II-28.

13. B. Davari, "Numerical study of viscous flows past a circular cylinder: application of Chorin's method" LBL-2480, UC-32 Mathematics and Computers TID-4500-R61.

LEGAL NOTICE

This report was prepared as an account of work sponsored by the United States Government. Neither the United States nor the United States Atomic Energy Commission, nor any of their employees, nor any of their contractors, subcontractors, or their employees, makes any warranty, express or implied, or assumes any legal liability or responsibility for the accuracy, completeness or usefulness of any information, apparatus, product or process disclosed, or represents that its use would not infringe privately owned rights.

TECHNICAL INFORMATION DIVISION
LAWRENCE BERKELEY LABORATORY
UNIVERSITY OF CALIFORNIA
BERKELEY, CALIFORNIA 94720